Hydrology and Earth System Sciences, 3(1), *71–84* (1999) © EGS

Hydrology & Earth System Sciences

A coupled dual source GCM SVAT

E.M. Blyth,[1] R.J. Harding[1] and R. Essery[2]

[1] Institute of Hydrology, Wallingford, Oxon OX10 8BB, UK
[2] Hadley Centre, Bracknell, Berks RG12 2SY, UK

Abstract

The single source SVAT scheme (MOSES) used in the UK Meteorological Office GCM is modified to include two sources. The performances of the original and the new scheme are then compared with minimal calibration against data from sparse vegetation taken from the HAPEX-Sahel experiment. Both schemes perform well; in particular the dual source SVAT successfully simulates the different temperatures of the sparse vegetation and soil. It is demonstrated that the two sources need to be coupled, rather than acting independently, for an accurate result. Some components of the single and dual source schemes are driven off-line by measured surface temperature. In this case a dual source SVAT scheme performs significantly better than a single source scheme.

Introduction

Arid and semiarid areas cover one third of the land surface of the earth (Verstraete and Schwartz, 1991). These regions are almost always covered with sparse vegetation. Very often they are regions where human and climatic pressures are causing land degradation, leading to a loss of vegetation cover and soil with possible feedbacks with the climate system (e.g. Xue and Shukla, 1993). Many General Circulation Models (GCMs), including the model used at the UK Meteorological Office, use single source surface schemes to represent land cover; that is they use one surface temperature per grid square. Previous work has shown that a single source model is inadequate to represent sparse vegetation and that two sources are needed (Harding *et al.*, 1997), one for soil and one for vegetation. The first land surface scheme to include two separate energy budgets for soil and vegetation was proposed by Deardorff (1978). There are now many dual source surface schemes in operation such as SiB (Sellers *et al.*, 1986), BEST (Pitman *et al.*, 1991) and CLASS (Verseghy *et al.*, 1993). This paper describes the transformation of the UK Meteorological Office's Surface Energy Balance Scheme (MOSES) from a single source into a dual source scheme, with a comparison of the two schemes in relation to data from sparse terrain.

The dual source scheme was proposed originally by Shuttleworth and Wallace (1985). It partitions the available energy into heat and moisture fluxes over two surfaces simultaneously using the Penman-Monteith equation. It has been used extensively to study data from sparse vegetation (Huntingford *et al.*, 1995 and Blyth and Harding, 1995). The original dual source scheme has the available energy as an input. However, in an operational scheme. the available energy is a function of the solution to the energy balance, via the surface temperature and the ground heat flux. MOSES includes the ground heat flux implicitly in the Penman-Monteith equation. The equations that include the ground heat flux implicitly in the available energy of the heat and moisture fluxes of the dual source model are presented here for the first time.

The single source and dual source models are both compared to data so that an assessment can be made of the benefits (or otherwise) of using a dual source model in the context of a GCM land surface scheme. Two forms of dual source model are tested; one where the fluxes from the soil and vegetation are coupled via an inter-canopy humidity deficit, and the other where the surfaces respond to the reference height humidity deficit only.

An off-line test of the components of the surface schemes, driven by observed temperatures, is used to explore the performance of the components of the scheme to a single source and a dual source representation of the surface temperature.

The SVAT

BASIC STRUCTURE

MOSES is the SVAT (Soil Vegetation Atmosphere Transfer) scheme developed for use in the UK Meteorological Office unified model. MOSES has a four

layer soil model with coupled heat and moisture fluxes. The evaporation is the sum of evaporation of intercepted water, transpiration and bare soil evaporation, the last two of which have surface resistances. Water for the transpiration is taken from the soil layers in which there are roots, the water for the bare soil evaporation is taken from the top soil layer and the water for the evaporation of intercepted water is taken from a canopy store. The two surface resistances increase and the area covered by water on the canopy decreases as the water available in the appropriate store reduces. Although there are three sources of evaporation, there is only one sensible heat flux, one aerodynamic resistance, one surface temperature and one net radiation for the composite surface. MOSES is therefore classed as a single source model.

To change MOSES into a dual source model, the radiation balance, aerodynamic resistance and surface temperature for the bare soil must be separated from that of the vegetation. The following text describes the alterations that were necessary to effect this change.

MOSES is based on the Penman-Monteith equation (Monteith, 1981) whereby the surface temperature is eliminated from the calculation of evaporation but can be diagnosed from the energy balance. The dual source model requires the same logic. There are two published methods which use the Penman-Monteith equation in a coupled dual source SVAT Shuttleworth and Wallace (1988) modelled one source above the other so that both sources cover the whole area but the lower source is partially shaded. Dolman (1993) and Huntingford *et al.*, (1995) modelled two sources side-by-side with full radiation loading on both sources, but only partial coverage. The objective in deriving the model presented here was to combine the two approaches so that there is a partial coverage of shady vegetation included within both the radiation and hydrology part of the model, as shown in Fig. 1.

RADIATION

Long wave radiation

In MOSES, the single surface temperature diagnosed at the previous timestep is used to estimate the net long wave radiation, L_1.

$$L_1 = L\downarrow - \sigma T_1^4 \qquad (1)$$

where $L\downarrow$ is the downward long wave radiation. T_1 is the surface temperature of the single source model and σ is Stefan-Boltzmann's constant. The emissivity is assumed to

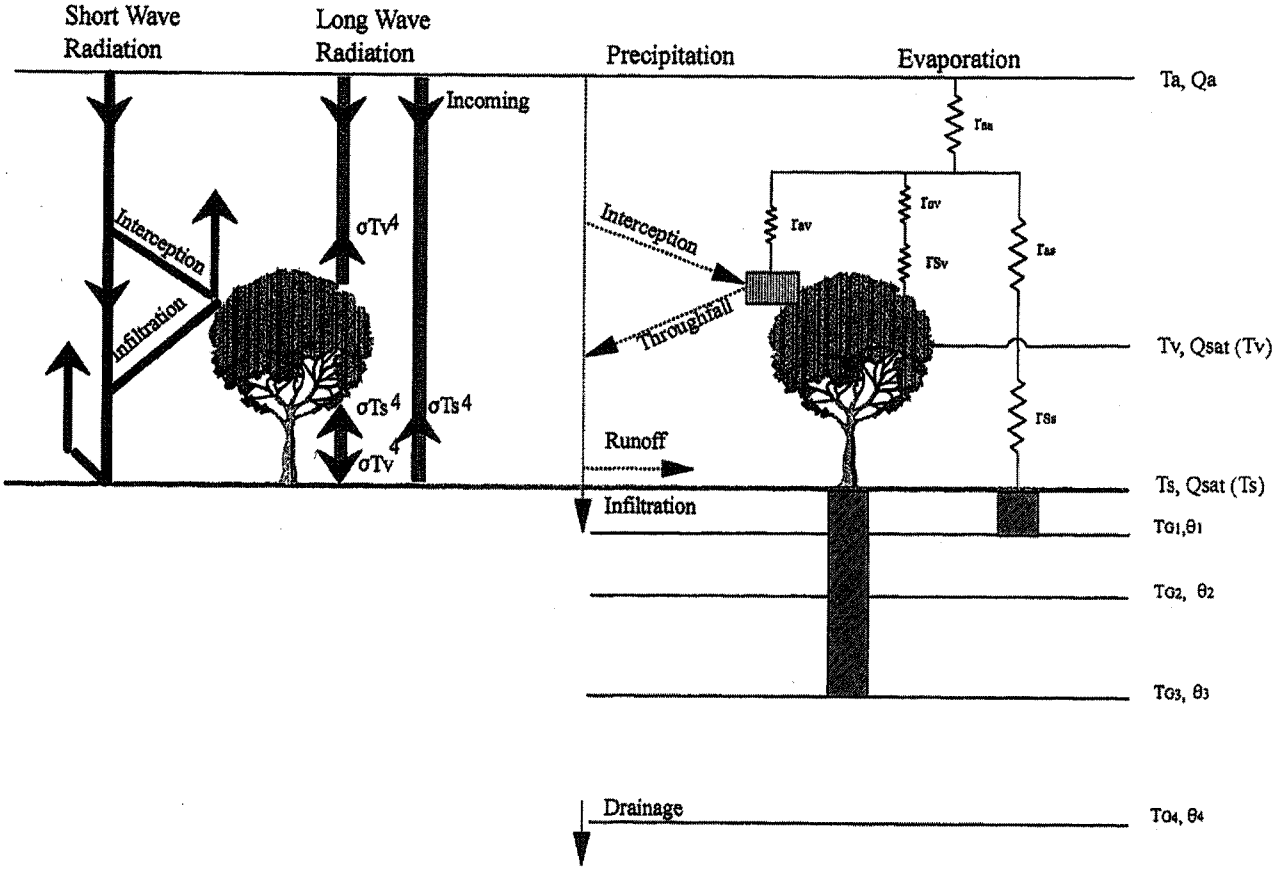

Fig. 1. *Schematic diagram of the coupled dual source SVAT scheme. The three shaded blocks represent the three sources of water (canopy interception, root-depth soil moisture for transpiration and top-layer soil moisture for bare soil evaporation).*

be unity. The definitions and units of all the variables are given in the Nomenclature in Appendix 1. The subscript s refers to soil, subscript v to vegetation and subscript 1 refers to the single source model.

For the new dual source version, soil and vegetation surface temperatures (T_s and T_v respectively) from the previous timestep are again used to calculate the outgoing long wave radiation from the soil and vegetation. In addition, there is an exchange of longwave radiation between the soil and the vegetation over the vegetated area. There is no filtering of the long wave radiation by the vegetation—it is all absorbed. The net long wave radiation for the soil and vegetation (L_s and L_v respectively) are given by the following equations.

$$L_s = (1 - V)L\downarrow + V\sigma T_v^4 - \sigma T_s^4 \quad (2)$$

$$L_v = L\downarrow + \sigma T_s^4 - 2\sigma T_v^4 \quad (3)$$

where V is the fraction of ground covered by vegetation. The radiation L_v is the value per unit area of vegetation, rather than per unit area of ground.

Short wave radiation

In MOSES the outgoing short wave radiation is a multiple of the incoming short wave radiation($S\downarrow$), hence the net short wave radiation, S_1 is given by

$$S_1 = S\downarrow (1 - \alpha_1) \quad (4)$$

In the dual source model the soil and vegetation have different values of albedo (α_s and α_v) and the incoming short wave radiation is attenuated by the canopy of the vegetation. This attenuation, X, is dependent on the Leaf Area Index (L^*), according to Beer's Law.

$$X = \exp(-0.7L^*) \quad (5)$$

where the value of 0.7 is taken from Shuttleworth and Wallace (1985).

Multiple reflections of the short wave radiation between the vegetation and the soil beneath the vegetation are also taken into account. Consideration of multiple reflections, and summing to infinity gives the following net short wave radiation for the soil and vegetation (S_s and S_v respectively):

$$S_s = \left[V\frac{X(1-\alpha_v)(1-\alpha_s)}{1-\alpha_v\alpha_s} + (1-v)(1-\alpha_s)\right]S\downarrow \quad (6)$$

$$S_v = \left[1-\alpha_v - \frac{X^2(1-\alpha_v)^2\alpha_s}{1-\alpha_v\alpha_s} - \frac{X(1-\alpha_v)(1-\alpha_s)}{1-\alpha_v\alpha_s}\right]S\downarrow \quad (7)$$

The derivation of Eqns. 6 and 7 is given in Appendix 2.

AERODYNAMIC RESISTANCES

The network of the aerodynamic resistances is shown in Fig. 1. The equations for the aerodynamic resistances have been simplified substantially from their previously published forms (see for example Huntingford *et al.*, 1995). Here roughness lengths are used rather than a fuller description of the scalar transports through the plant canopy (e.g. Raupach, 1987; Huntingford *et al.*, 1995). This more empirical approach has the advantage that the roughness lengths are known or can be estimated from characteristics of the surface. The disadvantage is that it is not physically correct to model the wind speed as a logarithmic profile through the canopy. However, as indicated by McNaughton and van den Hurk (1995), the turbulent transport beneath an overstorey canopy is poorly known. Therefore, a simple representation seems the most appropriate.

The new equations are as follows

$$r_{aa} = \frac{1}{ku*}\left(\ln\left(\frac{z_r}{z_0}\right) - \psi\right) \quad (8)$$

$$r_{av} = \frac{1}{ku*}\ln\left(\frac{z_0}{z_{0v}}\right) \quad (9)$$

$$r_{as} = \frac{1}{ku*}\ln\left(\frac{z_0}{z_{0s}}\right) \quad (10)$$

where the values of z_{0v} and z_{0s} are the scalar roughness lengths for vegetation and soil respectively. These values are obtained using the standard estimate of scalar roughness length in homogeneous terrain, of one tenth the value of momentum roughness length. k is von Karman's constant and u_* is the friction velocity. Thus, the values of r_{av} and r_{as} are the excess resistances of the vegetation and soil, while r_{aa} is the aerodynamic resistance for momentum and scalars from the reference height, z_r, down to the momentum roughness length, z_0. The intermediate height referred to by Huntingford *et al.* (1995) is taken here as the momentum roughness length of the site. ψ, the stability correction is calculated, as in MOSES, as a function of the vertical gradients of humidity, temperature and wind speed between the momentum roughness length, z_0 and the reference height z_r.

SURFACE RESISTANCES

The surface resistance sub-model in MOSES remains unchanged in the dual source model. A full description of this sub-model is given by Cox *et al.* (1998) and an outline follows to aid discussion in the later sections. The surface resistance, r_{Sv}, is a function of the photosynthetic activity of the plant, and it depends on soil moisture, radiation and temperature (T_1 for the single source model, T_v for the dual source model). There is a critical humidity deficit (D_C) and a critical temperature ($T_{\max}$). If the atmospheric values of temperature and humidity deficit rise above these critical points, then the surface resistance goes to infinity and transpiration stops. The values of the parameters in this model of stomatal resistance depend on the function type of the vegetation (C3 grass, C4 grass, needleleaf tree, broadleaf tree or shrub).

The soil is assumed to have a surface resistance, which is altered by a function dependent on the soil moisture in the top layer of the soil model. The parameters in this model of soil surface resistance depend on the soil type: sand, loam or clay.

SURFACE FLUXES OF HEAT AND MOISTURE

The equations for the calculation of surface fluxes of heat and moisture in MOSES are based on the Penman-Monteith equation. In this dual source scheme, the Penman-Monteith equation is applied from a point 'i'. The temperature and humidity deficit at this point (T_i and D_i) are interpolated from the temperature and humidity deficit at the reference height (T_a and D_a) using Eqns 15 and 16. This method follows Shuttleworth and Wallace (1985). In MOSES, to obtain the correct available energy, the ground heat flux, G, is included implicitly in the Penman-Monteith equation (see Cox *et al.*, 1999). The method is used here, and the terms which include the heat capacity factor, C, in Eqns. 11 and 13 are thus included. This inclusion of the ground heat flux term into the dual source equations of Shuttleworth and Wallace (1985) introduces the variable T_i to Eqns. 11 and 13. This makes their solution more complicated than the solution used by Shuttleworth and Wallace (1985). The new method of solution is shown in Appendix 3. The basic equations are as follows

$$\lambda E_s = \frac{\Delta(L_s + S_s - C(T_i - T_{Gl})) + D_i\left(\frac{\rho c_p}{r_{as}} + C\right)}{\Delta + \frac{c_p}{\lambda}(r_{as} + r_{Ss})\left(\frac{1}{r_{as}} + \frac{C}{\rho c_p}\right)} \quad (11)$$

$$\lambda E_v = V\frac{\Delta(S_v + L_v) + D_i\left(\frac{\rho c_p}{r_{av}}\right)}{\Delta + \frac{c_p}{\lambda}(r_{av} + r_{sv})\left(\frac{1}{r_{av}}\right)} \quad (12)$$

$$H_s \frac{\frac{c_p}{\lambda}(L_s + S_s - C(T_i - T_{Gl}))\frac{r_{as} + r_{Ss}}{r_{as}} - D_i\left(\frac{\rho c_p}{r_{as}}\right)}{\Delta + \frac{c_p}{\lambda}(r_{as} + r_{Ss})\left(\frac{1}{r_{as}} + \frac{C}{\rho c_p}\right)} \quad (13)$$

$$H_v = V\frac{\frac{c_p}{\lambda}(S_v + L_v)\frac{r_{av} + r_{Sv}}{r_{av}} - D_i\left(\frac{\rho c_p}{r_{av}}\right)}{\Delta + \frac{c_p}{\lambda}(r_{av} + r_{Sv})\left(\frac{1}{r_{av}}\right)} \quad (14)$$

where

$$D_i = D_a\left(\frac{\Delta(H_v + H_s)}{\rho c_p} - \frac{(\lambda E_v + \lambda E_v)}{\rho\lambda}\right)r_{aa} \quad (15)$$

$$T_i = T_a + \frac{H_v + H_s}{\rho c_p r_{aa}} \quad (16)$$

and

$$G + S_s + L_s - \lambda E_s - Hs \quad (17)$$

GROUND HEAT AND SOIL MOISTURE FLUX

The parts of MOSES that calculate the ground heat and soil moisture fluxes will not be described in detail here. Briefly, the value of the surface temperature, diagnosed from the energy balance, is used to update the soil temperatures using values of heat capacity and conductivity which are functions of the soil moisture. In MOSES, ground heat flux is driven by the single surface temperature. In the dual source version, it is driven by the soil surface temperature. The soil moisture model is unchanged. Parameters for the soil moisture and heat models depend on the soil type: sand, loam or clay.

HYDROLOGY

MOSES is designed to represent an area and so compensate for the fact that an areally averaged rainfall has a lower intensity than point rainfall. When the model is tested at a point using measured rainfall, this compensation has to be removed.

In addition, to convert the model for use with sparse vegetation, it was necessary to account for the vegetation fraction in the calculation of throughfall and runoff. The throughfall and runoff models are designed for full vegetation cover, so the first calculation is to divide the canopy water storage and capacity by the vegetation fraction. The usual calculations of throughfall and runoff are adjusted so that the exposed soil receives the full rainfall rate while the shaded soil receives the throughfall rate. The canopy water storage and capacity are returned to their area-average value by multiplying by the vegetation fraction.

Data

SITE DESCRIPTION

The data are from the fallow savannah site (13° 14.63'N, 2° 14.65'E) of the Southern Super-Site of HAPEX-Sahel (Goutorbe *et al.*, 1997). The description of the vegetation and soil types and of the data collected at this site is given by Wallace *et al.* (1994), but is summarised here. The site consists of a mixture of 2.3m high bushes and 0.7m high herbs on a sandy soil. Bushes occupy about 20% of the area and have a local leaf area index 2, while herbs, which occupy the rest of the area, have a leaf area index of 0.5. The roughness length for momentum was determined for a similar site by Lloyd *et al.* (1992) as z_{0m} = 0.17m.

MODEL PARAMETERS

Because the model allows only one vegetation type, model parameters need to be constructed to represent the combination of bushes and herbs. The area average vegetation fraction and leaf area index are required. Vegetation fraction is not a property that is usually measured, so it has to be inferred from the leaf area index. For the area covered by bushes, the leaf area index is 2 and the vegetation fraction is assumed to be 1. For the fraction of the ground covered in herbs, the leaf area index is 0.5. So the vegetation fraction is assumed to be 0.5 with a local leaf area index 1. This ties in with the fact that, according to Beer's law, a leaf area index of 1 gives 50% shade. The area average vegetation fraction is 20% of the bush and 80% of the herb fractions, giving a total vegetation fraction of 0.6. The area average local leaf area index of the vegetated fraction is one third bush and two thirds herbs, which is 1.33.

The albedo of bare soil was measured at a nearby site as 0.25. The albedo of the surface as a whole was measured previously over a similar site as 0.2 (Allen *et al.*, 1994). The albedo of the vegetation only was therefore set at 0.15.

The function type of the vegetation was taken as C3 grass. The soil type was sandy. The soil roughness in MOSES, set at 0.003 m, was left unchanged.

FLUX AND METEOROLOGICAL DATA

An overview of the experimental programme at the fallow savannah site is given by Wallace *et al.* (1994), but a brief summary follows. An Institute of Hydrology Mk 2 Hydra (Shuttleworth *et al.*, 1988) mounted at 9.5 m measured the hourly fluxes of the latent and sensible heat. The source area of the measurements is of the order of 1000 m^2 (Lloyd *et al.*, 1997). An automatic weather station measured the wind speed and direction, and the air temperature and humidity at a height of 5.4 m. The net radiation and the incoming and outgoing shortwave radiation were measured at several positions across the site. The data used in this paper are a spatial average of these radiation fluxes and so represent the surface as a whole. A tipping bucket rainguage measured the hourly rainfall rate at the site. The ground heat flux was measured with heat flux plates at a depth of 10 cm and corrected with temperatures measured at a depth of 5 cm.

The data cover the end of the wet season and the beginning of the dry down in 1992 (see Gash *et al.*, 1997 for a full description of the flux measurements and a comparison of the data from this site with the other HAPEX-Sahel sites). Figure 2 summarises the data. The daily values of evaporation and rainfall are given from day of the year 240 to 283 along with the specific humidity deficit of the air. The evaporation stays high throughout the period of study, despite the fact that the last 23 days are without rain, during which time the demand for evaporation increases as the air warms and dries.

The data were studied to check internal consistency. It was found that the area average net radiation measured from the 9 m tower balanced with the measured sensible and latent heat fluxes on a daily basis, with a random error of within 20 W m^{-2} averaged over the day. However, this measured net radiation was systematically about 15% less than the sum of the radiation components (calculated using a weighted average of the longwave and shortwave upward radiation components from the grass and bushes). It was not possible to identify which flux was at fault. The spatial heterogeneity of the surface means that the turbulent fluxes and net radiation may relate to a different grass/bush mix than the radiation components, which would introduce a systematic error. A data set was constructed from the measured data which had internal consistency by increasing the values of the net radiation, the sensible and latent heat fluxes by 15%, which is within experimental error (Lloyd *et al.*, 1997).

Measurements of the surface temperature were made over the bushes and over the herbs (at two sites). The bushes are dense enough to ensure that very little radiation from the soil is being sensed. The leaf area indices of the two herb sites are low enough for the measured temperature to be some combination of the soil temperature and the vegetation temperature. The true soil temperature will be a mix of hot exposed soil, cooler soil shaded by the herbs and even cooler soil shaded by the bushes. It is not possible to reconstruct an exact value of the soil surface temperature from the available measurements. In this paper, it will be assumed that the average temperature of the two herb sites represents the area average soil temperature.

Single and dual source SVATs driven with incoming long and short wave radiation and rainfall

CALIBRATION

The aim of this study was to run the models with minimal calibration. However, the values of T_{max} and D_C were such that the value of r_{Sv} was set to infinity in the afternoons of the last few weeks of the simulation. To allow the models to predict reasonable evaporation at this time it was necessary to lessen the temperature and humidity deficit control on the stomatal conductance. To this end, T_{max} and D_C were arbitrarily doubled from 36°C to 72°C and from 0.075 kg kg^{-1} to 0.15 kg kg^{-1} respectively (n.b. there is no T_{max} by Huntingford *et al.* (1995) and $DC = 0.15$ for all other function types). In addition, to improve the performance of the single source model, the value of the scalar roughness length was set at one thousandth of the momentum roughness length, as recommended for sparse terrain by several authors (Verhoef *et al.*, 1997; Stewart, 1995; Taylor *et al.*, 1997; Beljaars and Holtslag, 1991). Results

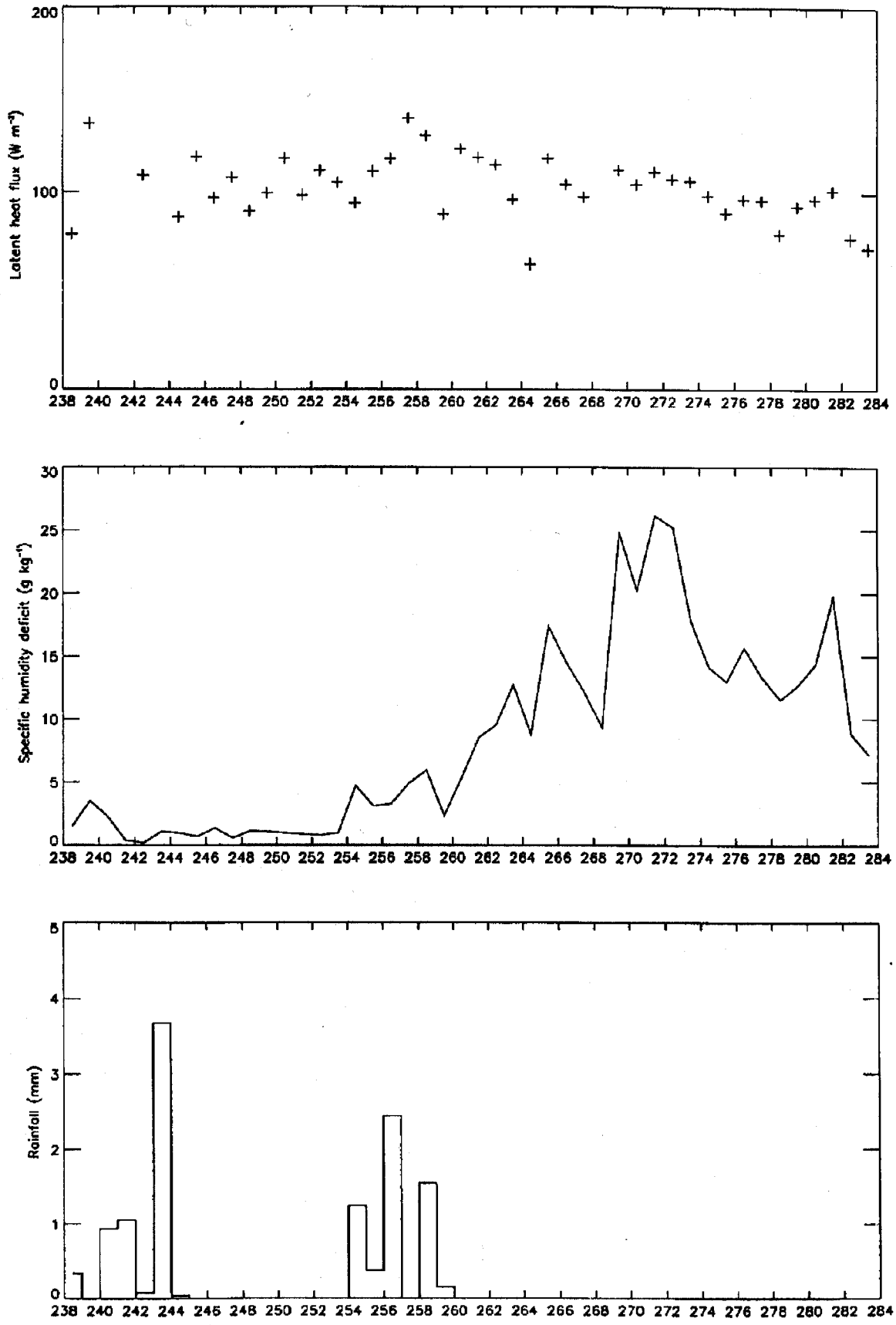

Fig. 2. *Observed daily average values of a) latent heat flux, b) humidity deficit and c) rainfall.*

with the standard value of scalar roughness length (one tenth of the momentum roughness length) are also shown.

COUPLED AND UNCOUPLED DUAL SOURCE MODELS

There are two types of dual source model; a coupled model where the turbulent fluxes from the two sources interact, and an uncoupled model where the fluxes are independent of each other. According to Blyth and Harding (1995), some coupling between the soil and vegetation to represent sparse vegetation in a dual source model allows sensible heat from the soil to flow into the vegetation, enhancing its evaporative flux. To assess whether this is the case at the fallow savannah site in this study, a simple, uncoupled dual source model is also tested against the data. This was done by setting $z_0 = z_r$ in the aerodynamic resistance Eqns. 8, 9 and 10.

RESULTS

Figures 3 and 4 show the daily average values of observed latent heat fluxes and net radiation respectively. The modelled values from the single source, the coupled dual source and the uncoupled dual source simulations are also shown. Figure 5 shows the surface temperatures, both observed and modelled by the single source and coupled dual source models. The uncoupled dual source model is not shown in this figure for clarity's sake. It has a similar form to the coupled dual source model, but the soil temperature is higher and the vegetation temperature is lower. The figures start ten days after the start of the simulation, thus avoiding most of the missing data days, and allowing the models some spin-up time.

Table 1 gives the average differences between the model and observations for the evaporation, the net radiation and

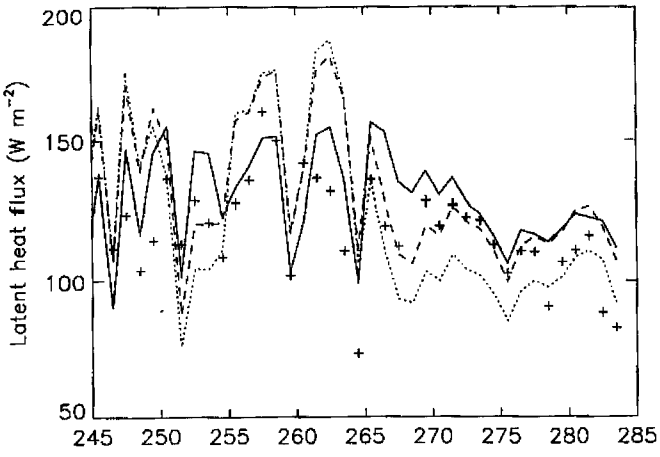

Fig. 3. *Daily average latent heat flux; observed (+), modelled by the single source model (solid line), the coupled dual source model (dashed line) and the uncoupled dual source model (dotted line).*

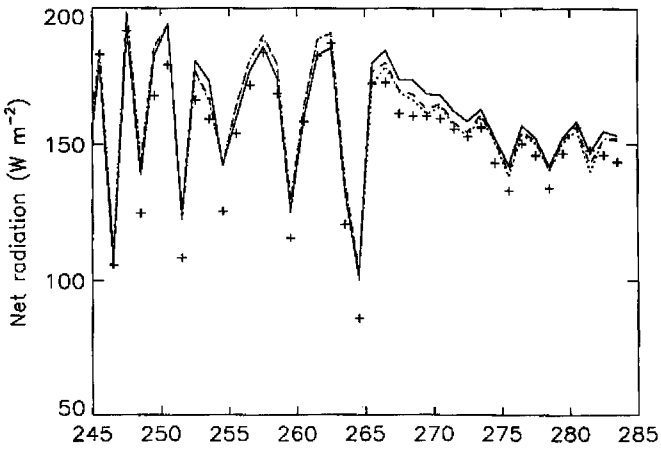

Fig. 4. *Daily average net radiation; observed (+), modelled by the single source model (solid line), the coupled dual source model (dashed line) and the uncoupled dual source model (dotted line)*

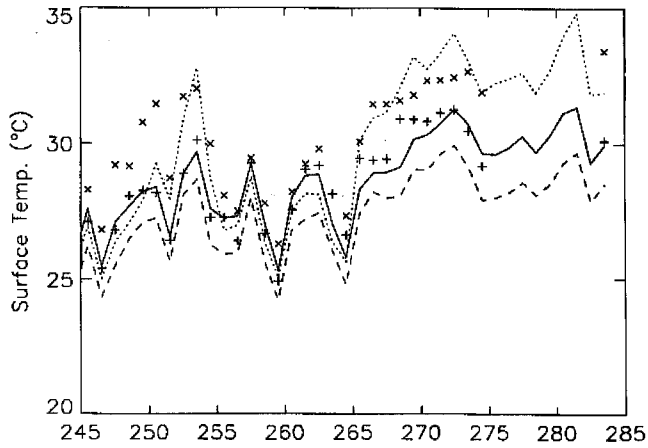

Fig. 5. *Daily average surface temperature; observed vegetation (+), observed soil (×), modelled by the single source model (solid line), and the coupled dual source model vegetation (dashed line) and soil (dotted line).*

the surface temperatures. The statistics have been quoted for two time periods with different hydrological regimes; day of the year 248 to 265 when there was plenty of rain and 266 to 283, when there was no rain and the soil dried out. The final statistic relates to the complete time period; day of the year 248 to 283.

The overall result is that all the models tend to overestimate evaporation, overestimate net radiation and underestimate the surface temperature. These errors are internally consistent (high evaporation rates cool the surface; this reduces the radiation loss and increases the energy available for evaporation). The error could be eradicated from all the models by calibration.

Another conclusion from the results shown in Table 1 is that the single source model which uses the original value of scalar roughness length is significantly worse than

Table 1. *Differences between modelled and observed latent heat, net radiation and surface temperature.*

	Day 248–265	Day 266–283	Day 248–283
Latent heat (Wm^{-2})			
Single source ($z_{0t} = z_0/10$)	+16.5	+15.6	+16.2
Single source ($z_{0I} = z_0/1000$)	+11.3	+14.1	+12.5
Coupled dual	+21.0	+5.7	+13.2
Uncoupled dual	+17.0	−10.5	+3.0
Net radiation (Wm^{-2})			
Single source ($z_{0t} = z_0/10$)	+14.6	+11.0	+12.7
Single source ($z_{0t} = z_0/1000$)	+9.4	+7.6	+8.5
Coupled dual	+11.4	+4.8	+8.1
Uncoupled dual	+10.8	+3.7	+7.2
Surface temp. (K)			
Single source ($z_{0t} = z_0/10$)	−1.2	−1.5	−1.4
Single source ($z_{0t} = z_0/1000$)	−0.7	−1.0	−0.9
Soil temp. (K)			
Coupled dual	−1.3	+0.5	−0.4
Uncoupled dual	−1.0	+1.3	+0.2
Veg. temp. (K)			
Coupled dual	−1.3	−1.7	−1.5
Uncoupled dual	−0.3	−2.0	−1.7

the other three models (errors are 50% greater). On the other hand, the other three models simulate fluxes that are similar to the observations, and there is not a big difference in their performance overall. A comparison of their performance in the two time periods is instructive.

In the first half of the period, all the models overestimate the evaporation. The single source model has the smallest error. It is possible that the soil evaporation is too high in the dual source models. This could result in their soil surface temperatures being too low.

For the second half of the period, the single source model overestimates the evaporation, the uncoupled dual source model underestimates it, while the coupled dual source model is close to the observations. The comparative success of the coupled dual source model over the uncoupled dual source model in this time period reflects the fact that the surface is acting as a coupled dual source, with sensible heat from the smooth, hot soil enhancing the evaporation from the rough, cool transpiring vegetation. It is for this situation that the coupled dual source model is designed. It is not surprising, therefore, that the uncoupled dual source model underestimates the evaporation, as it has no mechanism to transfer heat to the vegetation from the soil.

The comparative success of the coupled dual source model over the single source model is that its tendency to overestimate evaporation is offset by a reduction of the soil moisture, which occurs due to an overestimate of the evaporation in the first period.

The coupled dual source model splits the surface temperature into a value for the vegetation and one for the soil. Figure 5 shows that the two modelled temperatures are further apart than was observed (even more so in the case of the uncoupled source model), but the general trend has been captured.

In the dual source model there is only one soil surface temperature and one soil available energy whereas in practice the surface temperature of the shaded soil would be different from the surface temperature of the exposed soil. In effect, it is assumed that the soil surface temperature is a spatial average of the exposed and shaded soil temperatures. This is one of the grossest assumptions in the model, and is due for review.

Components of single and dual source SVATs driven with measured surface temperatures

DRIVING DATA AND METHOD

SVATs combine several components which interact. To ensure generality of the model, each of these components should model its process correctly. Unfortunately, even if

the predicted surface temperature and evaporation from a SVAT are correct, it is not necessarily the case that the components are correct, since the errors in one can be compensated for by the errors in another. In this section, the internal compensation that occurs within the single source SVAT as a result of using a single surface temperature is explored. Three components of the SVAT scheme are isolated and driven by the measured area average surface temperature and then by the appropriate surface temperature. The calibrated version of the SVATs from Section 4 is used in this section.

As an illustration of the diurnal variation of surface temperatures, Fig. 6a shows data for 28 September when the soil temperature reached 48°C and the maximum vegetation temperature was 37°C. The last rain in the area was 13 days before, so the soil evaporation is near zero. Therefore, on this day, the soil surface temperature is driven by the radiation balance and peaks at midday. The vegetation temperature is moderated by the transpiration, so it is lower than the soil temperature and it peaks later in the day at around 14.00.

LONG WAVE RADIATION

When the outgoing long wave radiation calculated using the average temperature (single source radiation) is compared with the average of the outgoing long wave radiation calculated with the separate temperatures (dual source radiation), the error is small. Figure 6b shows the difference for 28 September. Table 2 shows the maximum and mean differences from the whole time period and for 28 September. The dual source radiation is on average only 0.02% greater than the single source radiation. The daily maxima are on average 0.10% greater. For 28 September, the dual source radiation is 0.04% greater while the maximum is 0.22% greater than the single source radiation.

GROUND HEAT FLUX

The ground heat flux model from MOSES is used in this section to estimate ground heat flux, uncoupled from the soil moisture. Measured near-surface soil moisture, θ_1 is used to calculate the heat capacity, C_s, and the heat conductivity, K, according to the following equations

$$C_s = C_D + C_W\theta_1 \quad (18)$$

$$K = K_D + f\theta_1 \quad (19)$$

where C_D and C_W are the heat capacity of dry soil and water respectively. K_D is the conductivity of dry soil and f is the soil conductivity coefficient.

The near surface value of soil moisture was used in these calculations. The greatest temporal and spatial changes in temperature are near the surface, so it is this area which absorbs most of the energy.

The daytime ground heat flux predicted using soil temperatures (dual source ground heat) is greater than that predicted using the area average temperature (single source ground heat). Fig. 6c shows that the difference is large for 28 September. Table 2 shows that, on average, for hours when both fluxes were greater than 10 W m^{-2}, the dual source ground heat flux is 40% greater than the single source surface ground heat flux, while the day maxima are on average 55% greater. For 28 September, the dual source ground heat flux is 58% greater while the maximum is 72% greater than the single source ground heat flux.

STOMATAL CONDUCTANCE

The model of stomatal conductance (the reciprocal of stomatal resistance) has an explicit dependence on surface temperature and a dependence on surface humidity deficit, which has a strong temperature dependence.

The use of the average surface temperature underestimates the stomatal conductance (single source stomatal conductance) compared to the use of the vegetation temperature (dual source stomatal conductance). Figure 6d shows that the difference is significant for 28 September. Table 2 shows that the dual source stomatal conductance is 4.2% greater than the single source stomatal conductance while the average value of their daily maxima is 7.8% greater. For 28 September, the dual source conductances are 6.8% greater and the maximum is 8.5% greater than the single source conductances.

Conclusions

A coupled dual source structure has been implemented within an existing single source GCM land surface model

Table 2. *Percentage error in using mean surface temperature to calculate outgoing long wave radiation, ground heat flux and stomatal conductance.*

	28 September		Day 238–283	
	Maximum	Mean	Maximum	Mean
Outgoing long wave	+0.22	+0.04	+0.10	+0.02
Ground heat flux	+72	+58	+55	+40
Stomatal conductance	+8.5	+6.8	+7.8	+4.2

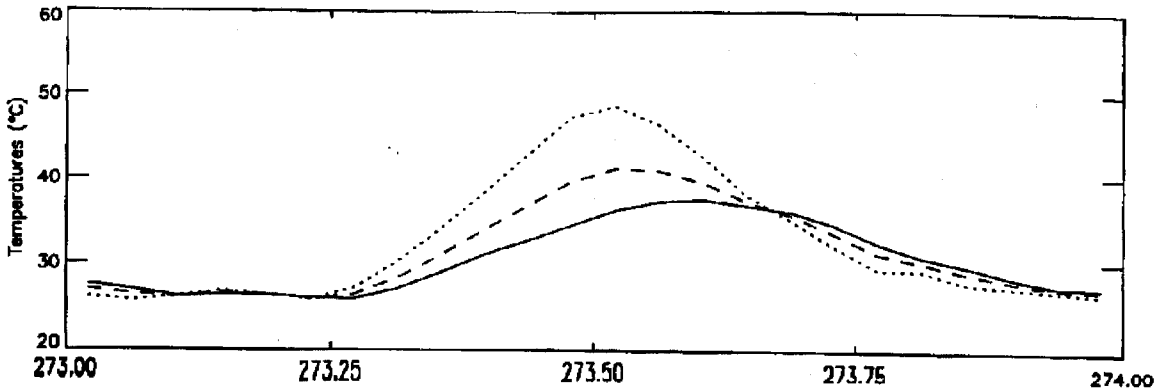

Fig. 6a. *Observed surface temperatures on 28 September for soil (dotted line), vegetation (solid line) and the area average (dashed line).*

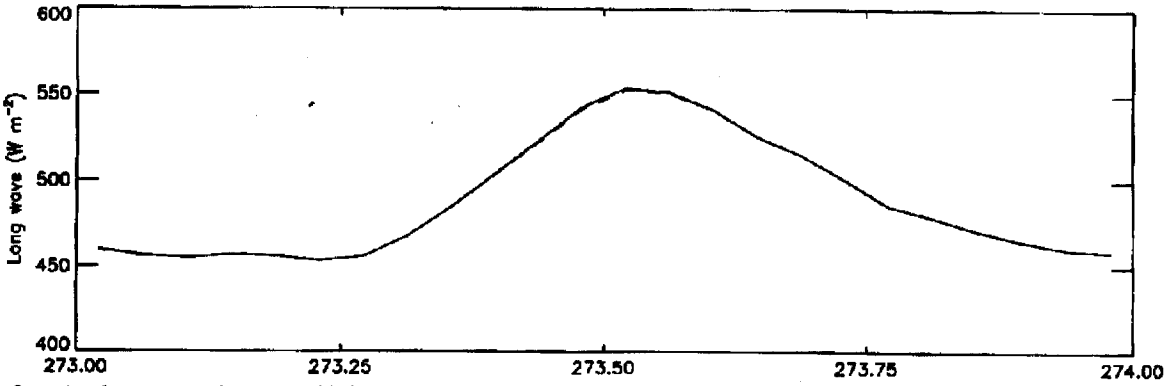

Fig. 6b. *Outgoing longwave radiation on 28 September predicted using area average surface temperature (dashed line) and using the area average of the temperature raised to the fourth power (solid line).*

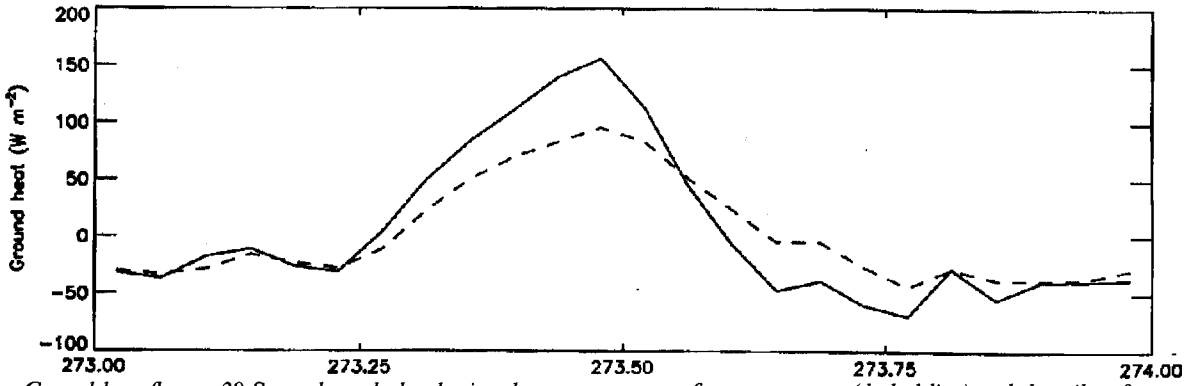

Fig. 6c. *Ground heat flux on 28 September calculated using the area average surface temperature (dashed line) and the soil surface temperature (solid line).*

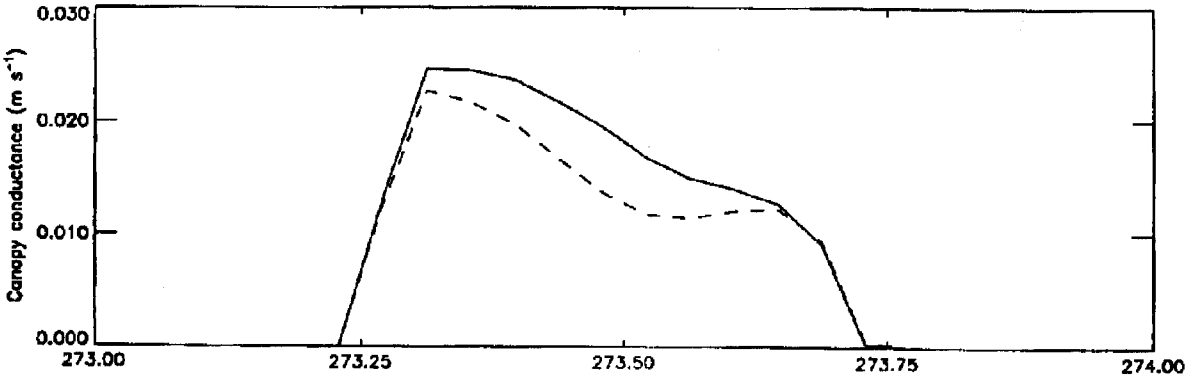

Fig. 6d. *Stomatal conductance on 28 September calculated using the area average surface temperature (dashed line) and the vegetation surface temperature (solid line).*

and both dual and single source versions have been tested against flux data from HAPEX-Sahel. When the SVAT is driven by the incoming net radiation and rainfall, both the single source model and the coupled dual source model give good estimates of the daily evaporation and area average surface temperature. However, to achieve a good fit for the single source model, a large, unrealistic ratio between the roughness lengths for momentum and heat (of 1000) is required. Blyth and Dolman (1995) showed that this ratio should not be expected to be a fixed quantity but will depend on the humidity deficit and available energy as well as the structure of the vegetation.This is a serious disadvantage of single source SVAT schemes when used with sparse vegetation. In contrast, the dual source structure enables the sparse nature of the vegetation to be included explicitly with the roughness lengths of heat and water vapour inferred from the characteristics of the surface. This is a considerable advantage for the implementation of a SVAT scheme within a GCM.

The uncoupled version of the dual source model gave a significantly worse fit to the observations. It appears from this result that the vegetation and soil need to be coupled together by aerodynamic resistances, rather than responding independently to the overlying atmosphere. The coupling allows for sensible heat to transfer from the soil to the transpiring vegetation, enhancing the evaporation (Blyth and Harding, 1995).

A second advantage of dual source structure is the explicit representation of two surface temperatures, for soil and vegetation. It is demonstrated that the use of a single surface temperature to represent a vegetation and soil surface can alter the calculation of stomatal resistance and ground heat flux if these are calculated in isolation from the rest of the SVAT. Although the single source model gave good results in terms of the evaporation and surface temperature, some internal compensating errors must have occurred, which implies that the calibrated single source model may not be transferable from one site to another. Other processes, such as soil respiration, are also strongly dependent on soil temperature. These are likely to be included within GCM land surface schemes in the near future and provide a further reason for including two sources within the model.

Both single source and dual source versions of the SVAT gave good predictions of the measured turbulent fluxes; mean errors are about 0.3 mm per day or 10% of the evaporation. The only minor calibration required was the modification of the temperature and humidity deficit responses of the conductance model. The uncertainty over the temperature and humidity deficit response highlights the crucial importance of the correct description of the conductance behaviour to the estimation of the energy balance in dry conditions and indicates a priority area for SVATs research in the future.

Acknowledgments

None of this work would have been possible without the use of the excellent HAPEX-Sahel dataset. The authors wish to thank all those involved in obtaining the data, in particular Colin Lloyd, Simon Allen, Cathy Holwill and Steve Gaze. E.M. Blyth and R.J. Harding acknowledge the financial support provided by the Natural Environment Research Council through its TIGER (Terrestrial Initiative in Global Environment Research) programme for both the data collection (award number GST/91/III.1)1A) and the modelling work (award number GST/91/III.2/1A). R. Essery was funded under the UK Department of Environment, Transport and Regions Climate Prediction Programme under contract PECD 7/12/37.

Appendix 1 Nomenclature and units

C	Heat capacity factor used in flux equations ($J\ s^{-1}\ m^{-2}\ K^{-1}$)
$C_{s,D,W}$	Heat capacity of soil, dry soil and water ($J\ kg^{-1}\ K^{-1}$)
c_p	Specific heat capacity of air ($J\ kg^{-1}\ K^{-1}$)
$D_{a,i}$	Specific humidity deficit of air at reference, intermediate height ($kg\ kg^{-1}$)
D_C	Critical humidity deficit ($kg\ kg^{-1}$)
$E_{s,v}$	Evaporation from the soil and vegetation ($mm\ s^{-1}$)
G	Soil heat flux ($W\ m^{-2}$)
$H_{s,v}$	Sensible heat flux for soil and vegetation components ($W\ m^{-2}$)
k	Von Karman's constant (0.4)
K	Heat conductivity of the soil ($J\ m\ s^{-1}$)
K_D	Heat conductivity of dry soil ($J\ m\ s^{-1}$)
L^*	Leaf area index
$L_{l,s,v}$	Net long wave radiation for single source, soil and vegetation ($W\ m^{-2}$)
$L\downarrow$	Downward long wave radiation ($W\ m^{-2}$)
f	Soil heat conductivity coefficient
$r_{aa,as,av}$	Aerodynamic resistances above canopy space from the canopy space to the soil, and to the vegetation (sm^{-1})
$r_{Ss,Sv}$	Surface resistances for soil and vegetation (sm^{-1})
$S_{l,s,v}$	Net short wave radiation for single source, soil and vegetation ($W\ m^{-2}$)
$S\downarrow$	Downward short wave radiation ($W\ m^{-2}$)
$T_{a,i}$ (K)	Air temperature at reference and intermediate height
$T_{l,s,v}$	Surface temperature: single source, soil and vegetation components (K)
T_{Gi}	Temperature below ground at level i (i = 1,4) (K)
T_{max}	Parameter in surface resistance model. (K)
u_*	Friction velocity ($m\ s^{-1}$)
V	Vegetation fraction
X	Fraction of radiation filtering through vegetation
z_r	Reference height (m)
$z_{0s,0v}$	Scalar roughness length of soil and vegetation components (m)
z_0	Momentum roughness length for the site (m)
$\alpha_{l,s,v}$	Albedo of single source, of soil and vegetation
Δ	Slope of saturated humidity curve with temperature ($kg\ kg^{-1}\ K^{-1}$)
$\lambda E_{s,v}$	Latent heat flux of soil and vegetation components ($W\ m^{-2}$)
ψ	Stability correction term

θ_1 Soil moisture content in top soil layer ($m^3\ m^{-3}$)
ρ Density of the air ($kg\ m^{-3}$)
σ Stefan Boltzmann constant ($W\ m^{-2}\ K^{-4}$)

Appendix 2 Calculation of net shortwave radiation

First reflection from the top of the canopy:

$$S{\uparrow}_{v_0} = \alpha_v S{\downarrow}$$

Shortwave radiation reaching soil surface after attenuation through vegetation;

$$S{\downarrow}_{S_0} = X(1 - \alpha_v)S{\downarrow}$$

Shortwave radiation reaching soil surface after n reflection from soil and vegetation;

$$S{\downarrow}_{S_n} = (\alpha_v\alpha_s)^n X(1 - \alpha_v)S{\downarrow}$$

Shortwave radiation leaving soil after n reflection from soil and vegetation;

$$S{\uparrow}_{S_n} = \alpha_s(\alpha_v\alpha_s)^n X(1 - \alpha_v)S{\downarrow}$$

Shortwave radiation leaving vegetation after n–1 reflections from vegetation, n reflections from soil and then transmission through vegetation;

$$S{\uparrow}_{V_n} = \alpha_s(\alpha_v\alpha_s)^{n-1}X^2(1 - \alpha_v)^2 S{\downarrow}$$

Then, summing $S{\downarrow}_{S_n}$ over an infinite number of reflections,

$$S_{\downarrow_s} = \frac{X(1-\alpha_c)}{1-\alpha_c\alpha_s} S_{\downarrow}$$

which gives a net radiation at the soil surface under the vegetation;

$$S_s = \frac{X(1-\alpha_s)(1-\alpha_v)}{1-\alpha_v\alpha_s} S_{\downarrow}$$

Summing $S{\uparrow}_{vn}$ over an infinite number of reflections gives the following;

$$S_{\uparrow_v} = \left[a_v + \frac{X^2(1-\alpha_v)^2\alpha_s}{1-\alpha_v\alpha_s}\right] S_{\downarrow}$$

So the net radiation at the vegetation surface is

$$S_v = \left[1-\alpha_v - \frac{X^2(1-\alpha_v)^2\alpha_s}{1-\alpha_v\alpha_s}\right] S_{\downarrow}$$

Appendix 3 Solution of surface flux equations

To solve the energy fluxes over two sources some more variables are defined, which are combinations of the resistances.

R_{SS} $1/(1 + r_{Ss}/r_{as})$ (dimensionless)

R_{SV} $1/(1 + r_{Sv}/r_{av})$ (dimensionless)

P_S $1([\lambda\Delta r_{as}/(r_{as} + r_{Ss}) + c_p + r_{as}C/\rho]$ $(K\ kg\ \mathcal{J}^{-1})$

P_V $1/[\lambda\Delta r_{av}/(r_{av} + r_{Sv}) + c_p]$ $(K\ kg\ \mathcal{J}^{-1})$

The equations are then as follows

$$E_s = R_{SS}\,P_S\,\{\Delta\,S_s + \Delta\,L_s - \Delta\,C(T_i - T_s) + D_i\,(c_p\,\rho/r_{as} + C)\}$$

$$E_v = V\,R_{SV}\,P_V\,\{\Delta\,S_v + \Delta L_v + D_i\,c_p\,\rho/r_{av}\}$$

$$H_s = c_p\,P_S\,\{S_s + L_s - C\,(T_i - T_s) - D_i\,\lambda\,R_{SS}\,\rho/r_{as}\}$$

$$H_v = V\,c_p\,P_v\,\{S_v + L_v - D_i\,\lambda\,R_{SV}\,\rho/r_{av}\}$$

$$E = E_s + E_v$$

$$H = H_s + H_v$$

$$T_i = T_a + Hr_{aa}/(c_p\,\rho)$$

$$D_i = D_a + (\Delta\,H/c_p - E)\,r_{aa}/\rho$$

Substituting these last two definitions into the equations for E_s, E_v, H_s, and H_v gives the following;

$$E_s = [R_{SS}\,P_S\,\{\Delta\,S_s + \Delta\,L_s - \Delta\,C\,(T_a - T_s) + D_a\,(c_p\,\rho/r_{as} + C)\}] + H\,[R_{SS}\,P_S\,\Delta r_{aa}/r_{as}] - E\,[R_{SS}\,P_S\,r_{aa}\,(c_p\,\rho/r_{as} + C)/\rho]$$

$$E_v = [V\,R_{SV}\,P_V\,\{\Delta\,S_v + \Delta L_v + D_a\,c_p\,\rho/r_{av}\}] + H\,[V\,R_{SV}\,P_V\,\Delta\,r_{aa}/r_{av}] - E\,[V\,R_{SV}\,P_V\,c_p\,r_{aa}/r_{av}]$$

$$H_s = c_p\,P_S\,(S_s + L_s - C\,(T_a - T_s) - D_a\,\lambda\,R_{SS}\,\rho/r_{as})] - H\,[P_S\,(C + \Delta\,\lambda\,R_{SS}\,\rho/r_{as})\,r_{aa}/\rho] + E\,[c_p\,P_S\,\lambda\,R_{SS}\,r_{aa}/r_{as}]$$

$$H_v = [V\,c_p\,P_v\,(S_v + L_v - D_a\,\lambda\,R_{SV}\,\rho/r_{av})] - H\,[V\,P_V\,\Delta\,\lambda\,R_{SV}\,r_{aa}/r_{av}] + E\,[V\,c_p\,P_V\,\lambda\,R_{SV}\,r_{aa}/r_{av}]$$

For clarity's sake, the groups in square brackets have been renamed. The terms in the first brackets of the E_s equation are called BE_s as shorthand for 'Basic E_s'. The group of terms in the next set of brackets is called E_sH to indicate that it is multiplied with the Heat term. The third group of terms is called E_sE to indicate that it is multiplied with the Evaporation term. The other equations are treated in the same way, so that the new set of equations is as follows;

$$E_s = BE_S + E_SH\,H - E_SE\,E$$

$$E_v = BE_V + E_VH\,H - E_VE\,E$$

$$H_s = BH_S - H_SH\,H + H_SE\,E$$

$$H_v = BH_V - H_VH\,H + H_VE\,E$$

Since $E = E_s + E_v$ and $H = H_s + H_v$ two simultaneous equations for E and H are given by

$$E\,(1 + E_SE + E_VE) = (BE_S + BE_V) + H\,(E_SH + E_VH)$$

$$H\,(1 + H_SH + H_VH) = (BH_S + BH_V) + E\,(H_SE + H_VE)$$

Which gives

$$E = ((1 + H_SH + H_VH)(BE_S + BE_V) + (E_SH + E_VH)(BH_S + BH_V))/R$$

$$H = ((1 + E_SE + E_VE)(BH_S + BH_V) + (H_SE + H_VE)(BE_S + BE_V))/R$$

where

$$R = (1 + E_SE + E_VE)(1 + H_SH + H_VH) - H_SE + H_VE)(E_SH + E_VH)$$

E and H are then substituted back into the equations for E_s, E_v, H_s, and H_v.

Implicit scheme in the two-source code

To solve the surface scheme simultaneously with the atmospheric model, the energy fluxes need to be calculated for a change in temperature and humidity at level 1, as a function of the old fluxes, the change in T and Q and the resistances. Some more definitions are used:

δT The change in temperature over one timestep (K),
δD The change in specific humidity in one timestep ($kg\ kg^{-1}$)
γ is the implicit weighting coefficient for ΔT and ΔD (=2) (dimensionless)

The new T_a' and D_a' are given by;

$$T_a' = T_a + \gamma\delta T$$

$$D_a' = D_a + \gamma(\delta D + \Delta\delta T)$$

If these are substituted into the equations for E_s, E_v, H_s and H_v, using the shorthand for the terms in the square brackets, to get E_s', E_v', H_s' and H_v' in terms of $E'(=E_s' + E_v')$ and $H'(=H_s' + H_v')$ we get

$$E_s' = BE_S + E_SH\ H' - E_SE\ E' - \gamma[R_{SS}\ P_S\ (\delta D\ (c_p\ \rho/r_{as} + C) - \delta T\ (c_p\ \Delta\ \rho/r_{as}))]$$

$$E_v' = BE_V + E_VH\ H' - E_VE\ E' - \gamma[V\ R_{SV}\ P_V\ (\delta D\ (c_p\ \rho/r_{av}) - \delta T\ (c_p\ \Delta\rho/r_{av}))]$$

$$H_s' = BH_S - H_SH\ H' + H_SE\ E' + \gamma[c_pP_S\ (\delta D\ (\lambda\ R_{SS}\ \rho/r_{as}) - \delta T\ (\Delta\lambda\ R_{SS}\ \rho/r_{as} + C))]$$

$$H_v' = BH_V - H_VH\ H' + H_VE\ E' + \gamma[V\ c_pP_V\ (\delta D(\lambda\ R_{SV}\ \rho/r_{av}) - \delta T\ (\Delta\lambda\ R_{SV}\ \rho/r_{av}))]$$

Shorthand is used again to represent the terms in brackets. So the group in square brackets in the E_s' equation is called E_SG to indicate that it is the Gamma terms in the E_s equation, and so on for the others.

After some manipulation, the solution for E' and H' can be found as follows:

$$E' = E - \gamma[((1 + H_SH + H_VH)(E_SG + E_VG) - (E_SH + E_VH)(H_SG + H_VG))/R]$$

$$H' = H - \gamma[((H_SE + H_VE)(E_SG + E_VG) - (1 + E_SE + E_VE)(H_SG + H_VG))/R]$$

Finally, if the terms in the square brackets of the E' equation are referred to as EG and the terms in the square brackets of H' equation as HG, to indicate that it is the Gamma term in the evaporation and heat equations respectively, then we can solve for E_s', E_v', H_s' and H_v' as follows

$$E_s' = E_s - \gamma(E_SH\ HG - E_SE\ EG + E_SG)$$

$$E_v' = Ev - \gamma(E_VH\ HG - E_VE\ EG + E_VG)$$

$$H_s' = H_s + \gamma(H_SH\ HG - H_SE\ EG + H_SG)$$

$$H_v' = H_v + \gamma(H_VH\ HG - H_VE\ EG + H_VG)$$

References

Allen, S.J., Wallace, J.S., Gash, J.H.C. and Sivakumar, M.V.K., 1994. Measurements of albedo variation over natural vegetation in the Sahel. *Int. J. Climatol.* **14**, 625–636.

Beljaars, A.C.M. and Holtslag, A.A.M., 1991. Flux parameterization over land surfaces for atmospheric models. *J. Appl. Meteorol.* **30**, 327–341.

Blyth, E.M. and Dolman A.J., 1995. The roughness length for heat of sparse vegetation. *J. Appl. Meteorol.* **34**, 583–585.

Blyth, E.M. and Harding R.J. 1995. Application of aggregation models to surface heat-flux from the sahelian tiger bush. *Agric. For. Meteorol.* **72**, 213–235.

Cox, P.M., Betts, R.A., Bunton, C., Essery, R.L.H., Rowntree, P.R. and Smith J., 1998a. The impact of new land surface physics on the GCM simulation of climate and climate sensitivity. *Climate Dynamics* in press.

Cox, P.M., Huntingford, C. and Harding, R.J., 1998. A canopy conductance and photosynthesis model for use in a GCM land surface scheme. *J. Hydrol.* **212–213**, 79–94.

Deardorff, J.W., 1978. Efficient prediction of ground surface temperature and moisture, with inclusion of a layer of vegetation. *J. Geophys. Res.* **83C**, 1889–1903.

Dolman, A.J., 1993. A multiple-source land surface energy balance model for use in general circulation models. *Agric. For. Meteorol.* **65**, 21–45.

Gash, J.H.C., Kabat, P., Monteny, B.A., Amadou, M., Bessemoulin, P., Billing, H., Blyth, E.M., deBruin, H.A.R., Elbers, J.A., Friborg, T., Harrison, G., Holwill, C.J., Lloyd, C.R., Lhomme, J.-P., Moncrieff, J.B., Puech, D., Soegaard, H., Taupin, J.D., Tuzet, A. and Verhoef, A., 1997. The variability of evaporation during the HAPEX-Sahel Intensive Observation Period. *J. Hydrol.* **188–189**, 385–399.

Goutorbe, J.-P., Lebel, T., Dolman, A.J., Gash, J.H.C., Kabat, P., Kerr, Y.H., Monteney, B., Prince, S., Stricker, J.N.M., Tinga, A. and Wallace, J.S., 1997. An overview of HAPEX-Sahel: A study in climate and desertification. *J. Hydrol.* **188–189**, 4–17.

Harding, R.J., Blyth, E.M. and Taylor, C.M., 1997. Issues in the aggregation of surface fluxes from a heterogeneous landscape: from sparse canopies up to the GCM grid scale. *Society for Experimental Biology seminar series*; **63**. Edited by P.R. van Gardingen, G.M. Goody and P.J. Curran.

Huntingford, C., Allen, S.J. and Harding, R.J., 1995. An intercomparison of single and dual-source vegetation-atmosphere transfer models applied to transpiration from sahelian savanah. *Boundary-Layer Meteorol.* **74**, 397–418.

Lloyd, C.R., Bessemoulin, P., Cropley, F.D., Culf, A.D., Dolman, A.J., Elbers, J., Heusinkveld, B., Moncreiff, J.B., Monteney, B. and Verhoef, A., 1997. A comparison of surface fluxes at the HAPEX-Sahel fallow bush sites. *J. Hydrol.* **188–189**, 400–425.

Lloyd, C.R., Gash, J.H.C. and Sivakumar, M.V.K., 1992. Derivation of the aerodynamic roughness parameters for a sahelian savannah site using the eddy correlation technique. *Boundary-Layer Meteorol.* **58**, 261–271.

McNaughton, K.G. and van den Hurk, B.J.J.M., 1995. A 'lagrangian' revision of the resistors in the two-layer model for calculating the energy budget of a plant canopy. *Boundary-Layer Meteorol.* **74**, 261–288.

Monteith, J.L., 1981. Evaporation and surface temperature. *Quart. J. Roy. Meteorol. Soc.* **107**, 1–27.

Pitman, A.J., Yang, Z.L., Cogley, J.G. and Henderson-Sellers, A., 1991. Description of bare essentials of surface transfer for the Bureau of Meteorology Research Centre AGCM. *Bur. Meteorol. Res. Rep.* **32**, 86pp.

Raupach, M.R., 1987. A Lagrangian analysis of scalar transfer in vegetation canopies. *Quart. J. Roy. Meteorol. Soc.* **113**, 107–120.

Sellers, P.J., Mintz, Y., Sud, Y.C. and Dalcher, A., 1986. A simple Biosphere Model (SiB) for use in general circulation models. *J. Atmos. Sci.* **43**, 505–531.

Shuttleworth, W.J. and Wallace, J.S., 1985. Evaporation from sparse crops—an energy combination theory. *Quart. J. Roy. Meteorol. Soc.* **111**, 839–855.

Shuttleworth, W.J., Gash, J.H.C., Lloyd, C.R., McNeill, D.D., Moore, C.J. and Wallace, J.S., 1988. An integrated micrometeorological system for evaporation measurement. *Agric. For. Meteorol.* **43**, 295–317.

Stewart, J.B., 1995. Turbulent surface fluxes derived from radiometric surface-temperature of sparse prairie grass. *J. Geophys. Res.-Atmospheres* **100**, 25429–25433.

Taylor, C.M., Harding, R.J., Thorpe, A.J. and Bessemoulin, P., 1997. A mesoscale simulation of land surface heterogeneity from HAPEX-Sahel. *J. Hydrol.* **189**, 1040–1066.

Verhoef, A., De Bruin, H.A.R. and van den Hurk, B.J.J.M., 1997. Some practical notes on the parameter kb(–1) for sparse vegetation. *J. Appl. Meteorol.* **36**, 560–572.

Verstraete, M.M. and Schwartz, S.A., 1991. Desertification and global change. *Vegetation.* **91**, 3–13.

Verseghy, D.L., Macfarlane, N.A. and Lazare, M., 1993. CLASS—a Canadian land-surface scheme for GCMs. 2. Vegetation model and coupled runs. *Int. J. Climatol.* **13**, 347–370.

Wallace, J.S., 1991. International workshop on soil-water balance in the Sudano-Sahelian zone—*IAHS publ.* **199**.

Wallace, J.S., Brouwer, J., Allen, S.J., Banthorpe, D., Blyth, E.M., Blyth, K., Bromley, J., Buerkert, A.C., Cantwell, M., Cooper, J.D., Cropley, F.D., Culf, A.D., Dolman, A.J., Dugdale, G., Gash, J.H.C., Harding, R.J., Harrison, R.G., Holwill, C.J., Jarvis, P.G., Levy, P.E., Lloyd, C.R., Malhi, Y.S., Massheder, J.M., Moncrieff, J.B., Pearson, D., Settle, J.J., Sewell, I.J., Sivakumar, M.V.K., Sudlow, J.D., Taylor, C.M. and Wilson, A.K., 1994. *HAPEX-Sahel Southern Super-Site Report*: An overview of the site and the experimental programme during the intensive observation period in 1992. Institute of Hydrology, Wallingford, UK. 55pp.

Xue, Y. and Shukla, J., 1993. The influence of land surface properties on Sahel climate. Part 1. Desertification. *J. Climatol.* **6**, 2232–2245.